

Design of Satellite Maneuvers for Inertia Parameter Estimation

Carlo Nainer^{*,**} Marion Gilson^{*} Hugues Garnier^{*}
Christelle Pittet^{**} H el ene Evain^{**}

^{*} *Universit e de Lorraine, CNRS, CRAN, F-54000 Nancy, France,
(e-mail: carlo.nainer,marion.gilson,hugues.garnier@univ-lorraine.fr).*

^{**} *CNES - The French Space Agency, F-31401 Toulouse, France,
(e-mail: christelle.pittet,helene.evain@cnes.fr)*

Abstract: This paper addresses the design of satellite maneuvers for the inertia estimation. The experiment design is an important step in system identification, since the choice of the excitation signal has a great influence on the precision of the parameter estimates. In order to design an optimal maneuver, the proposed method uses a cubic B-spline representation of the trajectory. The optimized maneuver is obtained through minimization of a functional based on the Fisher information matrix. The optimization process considers the physical constraints due to the saturation of the actuators. The effectiveness of the generated trajectory is evaluated via Monte Carlo simulations using the model of a satellite-type platform. Moreover, the optimized maneuver has been also tested on a real platform in a zero-gravity experiment where, due to the limited duration of the tests, the achievement of the maximum excitation is of great importance.

Keywords: Experiment Design, Aerospace, Satellites, Parameter Estimation, Flight Dynamics Identification

1. INTRODUCTION

An accurate model of spacecraft dynamics is necessary in order to guarantee a correct and fast control of the system. Many satellite parameters, such as inertia matrix and actuator alignment vectors, cannot be reliably estimated on ground. Therefore, several methods have been proposed in the literature in order to accurately estimate the parameter from the telemetry data (e.g. Norman et al. (2011); Yoon et al. (2017); Nainer et al. (2019)).

In the estimation process, one of the most important step is the experiment design. It consists in generating signals that well excite the system in order to obtain data with the highest information content. Several works studied the optimal excitation problem (Goodwin and Payne (1977); Armstrong (1989); Walter and Pronzato (1990); Franceschini and Macchietto (2008)), however, its application to the satellite parameter estimation is very recent. Weiss et al. (2015) propose a receding horizon optimization of the null motion in order to better estimate the reaction wheel alignments. In Sekhavat et al. (2009) the authors minimize the condition number of the regressor matrix to design the maneuver. Another approach is shown in Zhai et al. (2017), where a performance index similar to the condition number is used to optimize the maneuver to better estimate the satellite inertia matrix.

Even if the literature on satellite experiment design is quite limited, some related works can be found in the robotic field. Robot dynamics presents indeed many similarities with the rotational dynamics of satellites. Therefore many of these works can be easily adapted to the spacecraft case. In (Gautier and Khalil (1992)), the authors propose an

optimization based on a linear combination of the condition number and the equilibrium of the set of equations that generate the parameters. In (Swevers et al. (1997)), a D-optimality criterion on the Fisher information matrix is used, and the maneuvers are represented as a finite Fourier series, thus significantly reducing the number of parameters to be processed. A similar approach, still based on the finite Fourier representation, is proposed in (Park (2006)). In (Calafiore et al. (2001)), a genetic algorithm is used to determine excitation trajectories that minimize either the condition number of the regression matrix or the logarithmic determinant of the Fisher information matrix. A different maneuver parametrization is presented in (Rackl et al. (2012)), where B-splines are used. The cost function was based on a combination of the condition number and the sum of the joint torques (the latter term was included in order to improve the signal-to-noise ratio).

In this work, the experiment design problem for a small platform simulating a satellite behavior is considered. Since the platform is tested on a zero-G flight (Evain et al. (2019)), only very short maneuvers can be performed. For this main reason, a cubic spline parametrization is used since it allows for a fast and accurate derivative computation and oversampling. Different cost functions based on the Fisher information matrix are tested and compared. A prefilter is used in the experiment design process in order to tackle the non-ideality coming from the non-white noise source. The estimation improvements due to the maneuver design are demonstrated via Monte Carlo simulation and on a zero-G test on the real platform.

The paper is structured as follows. In Section 2, the satellite-platform dynamics is described as well as the

overall experiment design problem. The choice of the maneuver parametrization is shown in Section 3. In Section 4, the Fisher information based functionals are described, which include also the actuator constraints. Finally, the numerical simulations and the zero-G experiment results are presented in Section 5.

2. SATELLITE PLATFORM DYNAMICS AND PROBLEM STATEMENT

For testing purposes, we consider a satellite-type platform (Fig. 4), however, this work can be adapted to any satellite. The platform is equipped with a gyroscope for the angular velocity measurements and it uses 6 control moment gyros (CMGs) to generate the torque for the attitude control. The rotational dynamics in the body reference frame can be described by the Euler's equations (Sidi (1997)):

$$M(t) - \omega(t)^\times h_C(t) = J\dot{\omega} + \omega(t)^\times J\omega(t), \quad (1)$$

with

$$\omega(t)^\times = \begin{bmatrix} 0 & -\omega_z(t) & \omega_y(t) \\ \omega_z(t) & 0 & -\omega_x(t) \\ -\omega_y(t) & \omega_x(t) & 0 \end{bmatrix}, \quad (2)$$

where $M(t) \in \mathbb{R}^{3 \times 1}$ is the sum of the torques generated by the CMGs, $J \in \mathbb{R}^{3 \times 3}$ is the inertia matrix of the platform, $\omega(t) = [\omega_x(t), \omega_y(t), \omega_z(t)]^T \in \mathbb{R}^{3 \times 1}$ is the satellite angular rate, and $h_C(t)$ is the total angular momentum of the 6 CMGs. The torque $M(t)$ is directly related to their angular momentum derivative: $M(t) = -\dot{h}_C(t)$. The inertia J is a symmetric and positive definite matrix with the following form

$$J = \begin{bmatrix} J_{11} & J_{12} & J_{13} \\ J_{12} & J_{22} & J_{23} \\ J_{13} & J_{23} & J_{33} \end{bmatrix}. \quad (3)$$

The measurements $\bar{\omega}(t_k)$ of the angular velocity are assumed to be corrupted by a noise $\tilde{\omega}(t_k)$ as

$$\bar{\omega}(t_k) = \omega(t_k) + \tilde{\omega}(t_k), \quad (4)$$

where $\tilde{\omega}_x \sim \tilde{\omega}_y \sim \tilde{\omega}_z \sim N(0, \sigma^2)$. The drift term, typical of gyroscope sensors, has not been considered here since, due to the short experiment time (around 5 s), its effect would be negligible.

For the experiment design purpose, the 6 independent parameters of the inertia matrix are put into a vector: $\theta = [J_{11}, J_{22}, J_{33}, J_{23}, J_{13}, J_{12}]^T$ and (1) is rewritten as a linear function of the inertia parameters

$$M(t) - \omega(t)^\times h_C(t) = \left(\Gamma(\dot{\omega}(t)) + \omega(t)^\times \Gamma(\omega(t)) \right) \theta, \quad (5)$$

where the function $\Gamma(\cdot)$ is defined as

$$\Gamma(\omega) = \begin{bmatrix} \omega_x & 0 & 0 & 0 & \omega_z & \omega_y \\ 0 & \omega_y & 0 & \omega_z & 0 & \omega_x \\ 0 & 0 & \omega_z & \omega_y & \omega_x & 0 \end{bmatrix}. \quad (6)$$

Considering (4), (5) can be rewritten as function of the measured angular velocity $\bar{\omega}$

$$\underbrace{M(t) - \bar{\omega}(t)^\times h_C(t)}_{y(t)} = \underbrace{\left(\Gamma(\dot{\bar{\omega}}(t)) + \bar{\omega}(t)^\times \Gamma(\bar{\omega}(t)) \right)}_{\psi(t)} \theta + \nu(t), \quad (7)$$

where the term $\nu(t) \in \mathbb{R}^{3 \times 1}$ collects the overall noise effect.

We are now interested in the following problem: *Suppose we have an unbiased and consistent estimator for θ , find*

the excitation profile $\omega(t)$ that minimizes the variance of the estimate $\hat{\theta}$.

The experiment design presents three main steps

- (1) choose a suitable representation of the reference profile to be optimized,
- (2) build a functional to be minimized while including the system constraints,
- (3) select and apply an optimization solver.

3. MANEUVER PARAMETERIZATION

As it will be shown in the next section, the cost function to be minimized depends on the angular rate $\omega(t)$. Although also the torque $M(t)$ could be used to defined the maneuver, its use would become more complex. Several possible parametrizations exist for the representation of the reference profile $\omega(t)$. The simplest solution consists in optimizing a finite set of equispaced points of the maneuver, and interpolate a curve through them (Swevers et al. (1997)). Another approach consists in using a finite Fourier representation as in (Swevers et al. (1997); Park (2006)). With this parametrization the number of optimization parameters is significantly reduced and the derivative can be computed analytically, however the Fourier based representation is less flexible with respect to maneuver constraints. For example, in (Park (2006)), in order to guarantee predetermined initial and final conditions of the maneuver, a low order polynomial is added to the Fourier representation.

In this work, a cubic B-spline parametrization, similar to (Rackl et al. (2012)), is selected in order to make use of its interesting properties. Since in this work just short maneuvers are considered, the number of parameters required for this representation remains comparable with the ones of other less flexible methods. Splines are piecewise polynomials with pieces that are smoothly connected together. The joining points of the polynomials are called knots. An important property is that, in case of splines with uniform (and unit) knot spacing, we have

$$s_p(t) = \sum_k c_k \beta^n(t - k). \quad (8)$$

This means that a spline $s_p(t)$ can be expressed as a sum of integer shifts of a B-spline of degree n , denoted as β^n . A B-spline β^n is a symmetrical bell-shaped function obtained from a $(n + 1)$ -fold convolution of a rectangular pulse β^0 . Thanks to the representation defined in (8), each spline is defined by its sequence of coefficients c_k , which has the useful structure of a discrete signal even though the underlying model is continuous. Another interesting property of the splines is the so called convex hull property (Schumaker (2007)). This means that the curve lies in the convex hull defined by its control points. This property will be exploited in order to check the respect of the constraints also at intermediate points without interpolating the function values (if the control points respect the constraints, the whole curve will do). This choice leads to a theoretically conservative maneuver, but as it can be seen in Fig. 1, the allowed range has been widely exploited.

4. EXPERIMENT DESIGN

4.1 Fisher Information Matrix Based Experiment Design

The problem of finding good excitation trajectories is quite common in the field of parameter identification and different approaches have been presented in the literature. In system identification, an optimal design, in combination with an unbiased estimator, allows to minimize the variance of the estimates. An optimized experiment requires a lower number of runs (or shorter runs) to achieve a sufficient estimation precision. Intuitively, data with higher information content with respect to the parameters to be estimated should yield more precise estimates. This concept is represented by the Fisher information matrix (Goodwin and Payne (1977)), which is a measure of the amount of information that a measured variable x provides on the unknown parameter θ . It is formally defined as

$$I(\theta) = E[\nabla_{\theta} \log(p(x|\theta)) \nabla_{\theta} \log(p(x|\theta))^T], \quad (9)$$

or equivalently by

$$I(\theta) = -E[\nabla_{\theta}^2 \log(p(x|\theta))], \quad (10)$$

where $p(x|\theta)$ is the probability of the observed variable x for a given value of θ . In case of a linear regression model

$$y = \psi \theta + e, \quad (11)$$

where $y \in \mathbb{R}^{n \times 1}$, $\theta \in \mathbb{R}^{m \times 1}$, $\psi \in \mathbb{R}^{n \times m}$ and $e \in \mathbb{R}^{n \times 1}$ is a zero mean vector of independent identically distributed random variables with covariance matrix $\sigma^2 I$, it can be easily demonstrated that the Fisher information is given by (Ljung (1999), Ch.7 and Ch.13)

$$I(\theta) = \frac{\psi^T \psi}{\sigma^2}. \quad (12)$$

The Fisher information matrix is related to the Cramer-Rao lower bound (Kay (1998); Young (2011)). The Cramer-Rao inequality states that, for any unbiased estimator for θ , we have

$$\text{Var}(\hat{\theta}) \geq I(\theta)^{-1}. \quad (13)$$

The maximization of the Fisher information corresponds therefore to the minimization of the lower bound of the variance of the estimates.

Given N measurements, the least squares (LS) solution is

$$\hat{\theta}_{LS} = (\Psi^T \Psi)^{-1} \Psi^T Y, \quad (14)$$

where

$$Y = \begin{bmatrix} y(t_1) \\ y(t_2) \\ \vdots \\ y(t_N) \end{bmatrix}, \quad \Psi = \begin{bmatrix} \psi(t_1) \\ \psi(t_2) \\ \vdots \\ \psi(t_N) \end{bmatrix}, \quad (15)$$

and its parameter estimate has variance

$$\text{Var}(\hat{\theta}) = \sigma^2 (\Psi^T \Psi)^{-1}. \quad (16)$$

The Fisher information matrix, being the sum of the individual matrices, is given by

$$I(\theta) = \frac{\Psi^T \Psi}{\sigma^2}, \quad (17)$$

and it is therefore the inverse of the Fisher information. In the satellite application, the regressor $\psi(\bar{\omega})$ is correlated with the noise ν , and therefore a least squares method would yield biased estimates (Jun et al. (2010)). To obtain consistent parameter estimates, an instrumental variable (IV) method can be used (Söderström and Stoica (1983),

Young (2011), Nainer et al. (2019)). For the basic IV, the analytical solution is given by

$$\hat{\theta} = (Z^T \Psi)^{-1} Z^T Y, \quad (18)$$

where Z is an instrument, that should be correlated with the regressor Ψ and uncorrelated with the noise ν . Given (11), the IV parameter variance is

$$\text{Var}(\hat{\theta}_{IV}) = \sigma^2 (Z^T \Psi)^{-1} Z^T Z (\Psi^T Z)^{-1}. \quad (19)$$

Considering that the optimal instrument Z is the noise-free version of Ψ , (19) can be well approximated as

$$\text{Var}(\hat{\theta}_{IV}) \simeq \sigma^2 (Z^T Z)^{-1}, \quad (20)$$

and therefore, optimizing a functional based on (16) or (17) is effective also if the IV method is used. As a result, in the simple regression model (11), an optimal experiment design should maximize (17) or equivalently minimize (16).

Most of the design strategies that can be found in the literature have as objective the minimization of some functional $\rho(\text{Var}(\hat{\theta}))$. Among them, the most common criteria are (Walter and Pronzato (1990))

D-optimality: This optimality criterion requires to maximize the determinant of $\Psi^T \Psi$. Since the determinant is the product of the eigenvalues, which is inversely proportional to the product of the axes of the confidence ellipsoid, maximizing the determinant is equivalent to minimize the volume of the confidence ellipsoid of $\hat{\theta}$.

E-optimality: It requires the maximization of the smallest eigenvalue of the Fisher information matrix, equivalent to maximizing the minimum eigenvalue of $\Psi^T \Psi$. Geometrically, the E-optimal design minimizes the maximum diameter of the confidence ellipsoids of $\hat{\theta}$.

A-optimality: This criterion seeks to minimize the trace of $(\Psi^T \Psi)^{-1}$. It results in minimizing the average variance of the estimate $\hat{\theta}$.

Condition Number Minimization: This optimality criterion minimizes the condition number for inversion of the matrix $\Psi^T \Psi$. Since the condition number is not influenced by a scaling, the cost function must include a penalty in order to improve the signal to noise ratio.

4.2 Noise Model Correction Filter

Equation (16) assumes that $e(t)$ in (11) is a white noise. However, in the satellite model (7), the noise term $\nu(t)$ can be well approximated as

$$\nu \simeq (\gamma s + 1) e, \quad (21)$$

where e is a white noise source, γ is a scalar value and s is the differential operator (Nainer et al. (2019)). Therefore, optimizing a functional based on (16) does not generate an optimal maneuver. A solution consists in prefiltering (7): a low-pass filter $F(s) = \frac{1}{\gamma s + 1}$ is therefore applied to both sides of (7) to come up with

$$y_f(t) = \psi_f(t) \theta + \nu_f(t), \quad (22)$$

where $(\cdot)_f$ means that the signal is filtered by $F(s)$. For this filtered equation, the assumption of white noise ($\nu_f(t) \sim N(0, \sigma)$) is ‘‘approximately’’ fulfilled. Therefore, the scheme described in Section 4.1 can now be applied to (22) and the variance to be minimized becomes

$$\text{Var}(\hat{\theta}) = \sigma^2 (\Psi_f^T \Psi_f)^{-1}. \quad (23)$$

4.3 Including Physical Constraints in the Cost Function

Considering Section 4.1 and 4.2, the optimization consists in the minimization of a functional $\rho(\cdot)$ based on one of the possible criteria. For example, using the D-optimality criterion, the following cost function can be formulated

$$\rho_D = -\log\left(\det(\Psi_f(\omega, \dot{\omega})^T \Psi_f(\omega, \dot{\omega}))\right). \quad (24)$$

However, in addition to the minimization of the cost function, an optimal trajectory must also respect some physical constraints (e.g. saturation of the platform actuators). A simple solution consists in treating the system constraints as soft constraints, and therefore adding some penalty terms to the functional to be minimized that reach high values when close to the saturation/physical limits.

First, the actuator constraints should be converted into state constraints

$$|M_C(t)| \leq M_{max} \Rightarrow |\dot{\omega}(t)| \leq \dot{\omega}_{max}, \quad (25)$$

$$|h_C(t)| \leq h_{max} \Rightarrow |\omega(t)| \leq \omega_{max}. \quad (26)$$

Once the constraints are defined on ω and $\dot{\omega}$, the full cost function to be minimized, making use of (23), (25), (26), has the following form

$$\omega_{ref} = \arg \min_{\omega} \left(\rho\left(\Psi_f(\omega, \dot{\omega})^T \Psi_f(\omega, \dot{\omega})\right) + \text{penalty} \right), \quad (27)$$

where $\rho(\cdot)$ is a functional that will depend on the optimization criterion and the penalty, containing the physical limitation and the initial and final conditions of the maneuver, is defined as

$$\begin{aligned} \text{penalty} = & K_1(\omega(t_1) - \omega_{initial})^6 + K_1(\omega(t_N) - \omega_{final})^6 + \\ & + K_2 \sum [Q(\omega(t_k), \omega_{max}) + Q(-\omega(t_k), -\omega_{max})] + \\ & + K_3 \sum [Q(\dot{\omega}(t_k), \dot{\omega}_{max}) + Q(-\dot{\omega}(t_k), -\dot{\omega}_{max})], \end{aligned} \quad (28)$$

with

$$Q(x, \text{threshold}) = \begin{cases} 0 & x \leq \text{threshold} \\ (x - \text{threshold})^6 & x > \text{threshold} \end{cases}. \quad (29)$$

and where K_1 , K_2 and K_3 are some constants to weigh the different penalty terms. The summation in (28) should be extended to a thick grid of points in order to ensure that the constraints are respected for the whole signal. A better approach is to exploit the spline convex hull property and extend the summation for the penalty to the spline control points $\omega_{cp,k}$.

This nonconvex optimization problem can be solved using one of the available optimization tools. For this work we used the optimization toolbox from Matlab.

5. NUMERICAL AND EXPERIMENTAL RESULTS

To demonstrate the effectiveness of the maneuver design, the method is firstly tested via Monte Carlo simulation. Then, a real experiment is performed on a parabolic flight, where the platform is commanded with the optimized maneuver in a zero-G environment typical of a satellite.

5.1 Numerical Simulations

For the numerical simulations, the platform-satellite inertia J was set to

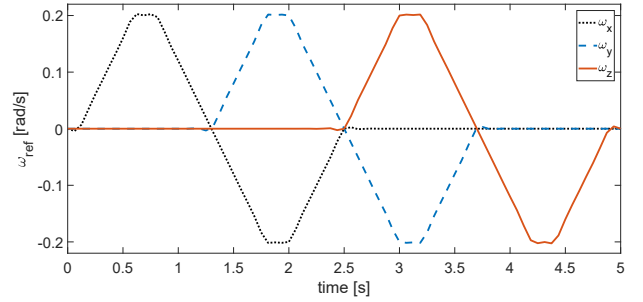


Fig. 1. Initial reference profile used for the optimization.

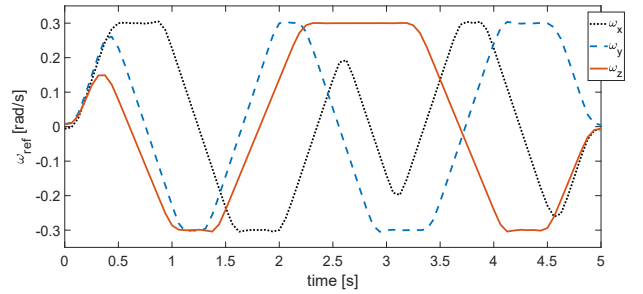


Fig. 2. D-opt maneuver.

$$\begin{bmatrix} 0.022 & 0 & 0 \\ 0 & 0.022 & 0 \\ 0 & 0 & 0.027 \end{bmatrix} [kg m^2], \quad (30)$$

and the CMGs saturation limits have been set to

$$\begin{cases} M_{C,x} \leq 0.040 Nm \\ M_{C,y} \leq 0.040 Nm \\ M_{C,z} \leq 0.047 Nm \end{cases} \quad \begin{cases} h_{C,x} \leq 0.0210 Nms \\ h_{C,y} \leq 0.0210 Nms \\ h_{C,z} \leq 0.0254 Nms \end{cases}. \quad (31)$$

The initial and final angular velocity for the maneuver were set equal to zero, while the experiment duration was set to 5 s. Fig. 1 shows the basic reference profile used as initial maneuver for the optimization algorithm. The choice of this initial profile was based on the two main conditions in order to avoid close to singular regressor: all three axes should be excited and the maneuvers should not be the same on different axes. The prefilter was set as

$$F(s) = \frac{1}{\gamma s + 1}, \quad (32)$$

where $\gamma = 0.8$. With a posteriori check we have verified that, with this value of γ , the error ν_f becomes reasonably white. Firstly, all the different criteria (see Section 4.1) have been tested and compared. The main criterion parameters of the different maneuvers are shown in Table 1, where it is clearly visible how the optimized maneuvers have better “criterion” values with respect to the basic profile. On the other hand, for this particular application, the different optimization criteria do not yield significantly different maneuver “properties”.

The practical advantage of the experiment design has been studied via Monte Carlo simulations, where the satellite inertia has been estimated both from the basic and the optimized reference profile. Additionally, also a scaled version of the basic profile is used in order to have the same maximum angular velocity ω amplitude compared to the optimized maneuver ($|\omega_{max}| \simeq 0.3 rad/s$). This “scaled” maneuver (ω_{ref}^*) is simply the basic maneuver of Fig. 1 multiplied by 1.5 ($\omega_{ref}^* = 1.5 \cdot \omega_{ref}$). Since there is very

Table 1. Main parameters for different optimality criteria. The arrows indicate whether a large \uparrow or small \downarrow value is better.

| | min. \uparrow eig. value | trace \downarrow | det. \uparrow | cond. \downarrow number |
|-----------------------|-------------------------------|--------------------|-----------------|------------------------------|
| basic | 0.099 | 21.27 | 0.0036 | 3.271 |
| A-opt | 1.663 | 2.431 | 330.6 | 1.546 |
| D-opt | 1.683 | 2.434 | 331.3 | 1.568 |
| E-opt | 1.746 | 2.528 | 253.8 | 1.465 |
| C.N ^o -opt | 1.532 | 2.883 | 115.3 | 1.426 |

Table 2. Inertia estimates from the different reference profiles [$10^{-3}kg m^2$]

| | J_{11} | J_{22} | J_{33} | J_{23} | J_{13} | J_{12} | |
|--------|----------|----------|----------|----------|----------|----------|------|
| basic | avg. | 22.24 | 22.33 | 27.30 | 0.14 | 0.12 | 0.15 |
| | st.d. | 1.12 | 1.67 | 1.30 | 1.27 | 1.01 | 1.20 |
| scaled | avg. | 22.14 | 22.15 | 27.15 | 0.05 | 0.05 | 0.05 |
| | st.d. | 0.67 | 0.96 | 0.76 | 0.74 | 0.60 | 0.69 |
| D-opt | avg. | 22.12 | 22.11 | 27.02 | 0.04 | 0.10 | 0.01 |
| | st.d. | 0.38 | 0.33 | 0.35 | 0.23 | 0.24 | 0.28 |
| true | 22.00 | 22.00 | 27.00 | 0.00 | 0.00 | 0.00 | |

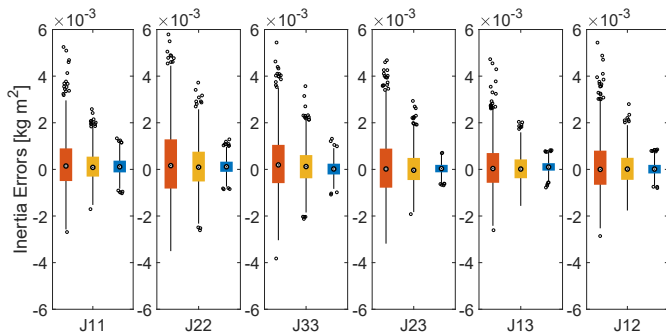


Fig. 3. Box plot for the inertia estimate errors. In red the results from the basic profile, in yellow the ones from the scaled basic profile, and in blue the D-opt profile.

little difference among the different optimization criteria, only the D-opt maneuver has been used (Fig. 2) in this comparison. The noise standard deviation on the angular velocity measurement was set as $\sigma = 0.025 rad/s$ for each of the three axes. As mentioned in Section 4, since the regressor $\psi(\bar{\omega})$ is correlated with the noise ν (Jun et al. (2010)), an IV method has been used to obtain consistent estimates of the inertia parameters (Nainer et al. (2019)). The results from a Monte Carlo simulation of 100 runs are shown in Table 2 and in Fig. 3. The increase of accuracy with the optimized reference profile is significant as it can be observed from the much smaller standard deviation in all the parameter estimates.

5.2 Zero-Gravity Experiment

Experiments have been performed on a real platform developed by ISAE-SUPAERO and ONERA (Fig. 4). The platform, named SCRAT-0g, has been tested on a parabolic flight that simulated a close to zero gravity environment. The purpose of this experiment was to test a satellite attitude controller on a platform which simulates a real satellite. The test has been repeated a few times, collecting the values of angular rate (from the gyroscope) and actuator angular momentum (generated by the 6 CMGs) at a sample rate of $16Hz$. The gyroscope white



Fig. 4. A picture of the SCRAT-0g platform tested on a parabolic flight (courtesy of ISAE SUPAERO and ONERA).

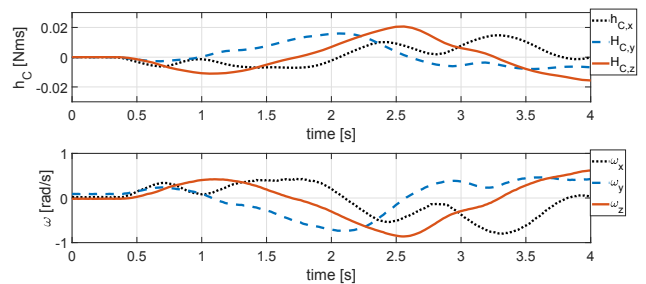


Fig. 5. Input-Output data from the zero-G experiment.

Table 3. Inertia Estimate from zero-G test

| | J_{11} | J_{22} | J_{33} | J_{23} | J_{13} | J_{12} |
|------------------------------------|----------|----------|----------|----------|----------|----------|
| $\hat{\theta}$ [$10^{-3}kg m^2$] | 20.04 | 21.26 | 25.75 | 0.09 | 0.04 | 1.08 |
| θ_{CAD} [$10^{-3}kg m^2$] | 20.80 | 20.80 | 26.00 | 0 | 0 | 0 |

noise had a standard deviation of $\sigma = 0.095^\circ/s$ on each axis. The experiment was in free floating, therefore, after the platform release, the unavoidable relative motion with respect to the airplane caused premature collisions with the inner walls. Since the final part of the maneuver was unusable, it was necessary to truncate the data. For the inertia estimation, 5 experiment data have been used, with a duration that varied from 2s up to around 4s. The input-output data of the longest achieved experiment is shown in Fig. 5. As for the simulation case, the inertia has been estimated by an instrumental variable method with a prefilter to deal with the derivatives in the system equation and its effect on the noise. The final inertia has been computed as a weighted average of the 5 different estimates (Ljung (1999), Ch.14):

$$\hat{\theta} = P \sum_i^n (P^{(i)})^{-1} \hat{\theta}^{(i)}, \quad P = \left(\sum_i^n (P^{(i)})^{-1} \right)^{-1}, \quad (33)$$

where $\hat{\theta}^{(i)}$ is the i -th inertia estimate and $P^{(i)}$ is its corresponding covariance. The weighted average inertia estimates, compared with the values of the CAD (computer-aided design) model, are shown in Table 3.

In this case we do not have a true value for comparison as for the simulations, but the inertia estimate is reasonably close to the nominal CAD values. Introducing the estimated parameters in (7), it is possible to do a cross validation by comparing the total torque ($M - \omega \times h_C$)

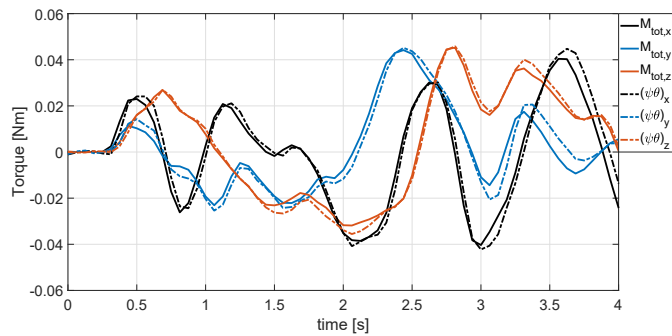


Fig. 6. Torque cross-validation: measured (solid lines), “estimated” (dash-dot line).

with their effect on the system ($\psi\hat{\theta}$). This comparison is depicted in Fig. 6, which shows a good match among the signals. Both the experiment design and the inertia estimate can be considered satisfactory, especially considering the very short duration of the experiments.

6. CONCLUSION

In this work we addressed the problem of finding optimal excitation maneuvers for the estimation of satellite inertia parameters. After a B-spline signal representation was introduced, a constrained nonlinear optimization was formulated to generate the excitation maneuver. The performance and practicability of the proposed approach has been tested both through numerical simulations and in a real experiment on a parabolic flight. The estimation results demonstrate the effectiveness of the optimized maneuver. Future works will consider the experiment design for a typical satellite that allows for longer maneuvers, as well as the use of null space excitation of the actuators to better estimate the actuator alignments.

ACKNOWLEDGEMENTS

We want to thank Louis Dubois, intern at CNES, for testing the designed maneuver on the parabolic flight.

REFERENCES

Armstrong, B. (1989). On finding exciting trajectories for identification experiments involving systems with nonlinear dynamics. *The International journal of robotics research*, 8(6), 28–48.

Calafiore, G., Indri, M., and Bona, B. (2001). Robot dynamic calibration: Optimal excitation trajectories and experimental parameter estimation. *Journal of robotic systems*, 18(2), 55–68.

Evain, H., Alazard, D., Rognant, M., Solatges, T., Brunet, A., Mignot, J., Rodriguez, N., and Dias-Ribeiro, A. (2019). Satellite attitude control with a six-control moment gyro cluster tested under microgravity conditions. *International Symposium on Space Flight Dynamics*.

Franceschini, G. and Macchietto, S. (2008). Model-based design of experiments for parameter precision: State of the art. *Chemical Engineering Science*, 63(19), 4846–4872.

Gautier, M. and Khalil, W. (1992). Exciting trajectories for the identification of base inertial parameters of

robots. *The International journal of robotics research*, 11(4), 362–375.

Goodwin, G.C. and Payne, R.L. (1977). *Dynamic system identification: experiment design and data analysis*. Academic press.

Jun, B.E., Bernstein, D.S., and McClamroch, N.H. (2010). Identification of the inertia matrix of a rotating body based on errors-in-variables models. *International Journal of Adaptive Control and Signal Processing*, 24(3), 203–210.

Kay, S.M. (1998). *Estimation theory*. Prentice Hall PTR.

Ljung, L. (1999). *System identification: Theory for the user*. Prentice-Hall, 2nd edition.

Nainer, C., Garnier, H., Gilson, M., Evain, H., and Pittet, C. (2019). In-flight inertia matrix estimation of a gyroless satellite. *5th CEAS Conference on Guidance Navigation and Control*.

Norman, M.C., Peck, M.A., and O’shaughnessy, D.J. (2011). In-orbit estimation of inertia and momentum-actuator alignment parameters. *Journal of Guidance, Control and Dynamics*, 34(6), 1798–1814.

Park, K.J. (2006). Fourier-based optimal excitation trajectories for the dynamic identification of robots. *Robotica*, 24(5), 625–633.

Rackl, W., Lampariello, R., and Hirzinger, G. (2012). Robot excitation trajectories for dynamic parameter estimation using optimized B-splines. In *2012 IEEE international conference on robotics and automation*, 2042–2047. IEEE.

Schumaker, L. (2007). *Spline functions: basic theory*. Cambridge University Press.

Sekhvat, P., Karpenko, M., and Ross, I. (2009). UKF-based spacecraft parameter estimation using optimal excitation. In *AIAA Guidance, Navigation, and Control Conference*, 5786.

Sidi, M.J. (1997). *Spacecraft dynamics and control: a practical engineering approach*, volume 7. Cambridge university press.

Söderström, T. and Stoica, P. (1983). *Instrumental variable methods for system identification, Lectures Notes in Control and Information Sciences*. Springer-Verlag.

Swevers, J., Ganseman, C., Tukul, D.B., De Schutter, J., and Van Brussel, H. (1997). Optimal robot excitation and identification. *IEEE transactions on robotics and automation*, 13(5), 730–740.

Walter, É. and Pronzato, L. (1990). Qualitative and quantitative experiment design for phenomenological models - a survey. *Automatica*, 26(2), 195–213.

Weiss, A., Leve, F., Kolmanovsky, I.V., and Jah, M. (2015). Reaction wheel parameter identification and control through receding horizon-based null motion excitation. In *Advances in Estimation, Navigation, and Spacecraft Control*, 477–494. Springer.

Yoon, H., Riesing, K.M., and Cahoy, K. (2017). Kalman filtering for attitude and parameter estimation of nanosatellites without gyroscopes. *Journal of Guidance, Control, and Dynamics*, 40(9), 2272–2288.

Young, P.C. (2011). *Recursive estimation and time-series analysis: An introduction for the student and practitioner*. Springer, 2nd edition.

Zhai, K., Wang, T., and Meng, D. (2017). Optimal excitation design for identifying inertia parameters of spacecraft. *Acta Astronautica*, 140, 370–379.